Numerical Calculation of the Dielectric Spectra of Cell-Type Particles

Viviana Zimmerman*,† and Constantino Grosse†,‡

Departamento de Fısica, Universidad Nacional de Tucumán, Av. Independencia 1800, (4000) S.M. de Tucumán, Argentina, and Consejo Nacional de Investigaciones Cientıficas y Técnicas, Argentina

Received: March 18, 2004; In Final Form: May 26, 2004

Dielectric spectra of a suspension of cells in electrolyte solution and dipole coefficient spectra induced by an AC electric field are numerically calculated using a network simulation method. The cell model consists of a conducting internal medium surrounded by an insulating membrane and by a charged permeable cell wall. The dependence of the low-frequency dielectric spectra with the internal medium properties is analyzed.

1. Introduction

The electrokinetic behavior of cell suspensions has been widely studied both experimental and theoretically in the high-frequency range, where the dispersions related to the conductivity and permittivity differences between the media that constitute the system occur.[1−9] However, the low frequency dielectric behavior (that is in the frequency range related to the double layer polarization) has been mainly studied experimentally.[2,7,10−14] As for the few theoretical studies, it was generally assumed that the low frequency behavior does not depend on the internal composition of the dispersed particle, but only on its ζ-potential, so that the theories developed for homogeneous particles can also be used for cells.[2,13−15]

This hypothesis was analyzed in a previous paper,[16] where the dipole coefficient spectra of cells with different internal medium properties were numerically calculated. It was found that the low-frequency behavior of the dipole coefficient is indeed independent of the internal medium properties if the charge of the cell is kept constant. In the present work, the same hypotheses are reconsidered, analyzing in this case the dependence of dielectric spectra of cell suspensions with the internal medium properties. In contrast with the preceding results, it is shown that the low frequency dielectric spectra of cells are mainly determined by the internal medium properties, unless the particle is highly charged and the double layer sufficiently thin.

The cell model is the same as the one considered in the preceding paper,[16] and it consists of a conducting internal medium surrounded by an insulating membrane and a charged permeable cell wall. The permittivity and conductivity of the cell suspension are calculated numerically using a network simulation method. This method has been successfully applied over the past few years to study different aspects of the dielectric and electrokinetic properties of electrolyte solutions and colloidal systems,[17−20] and was recently applied to the prediction of electrorotation spectra of latex type particles,[21] and cells.[16] The procedure consists of discretizing the domain and the differential equations, as in the linear finite difference method, and establishing the similitude between the discretizated equations inside every differential region and the equations that represent an elementary electric circuit composed of basic electronic components (resistors, capacitors, and current and voltage sources). Hence, the solution of the original problem is reduced to the solution of potentials and currents in a network composed of a set of these elementary subcircuits. The direct solution of the governing differential equations is thus avoided, and any commercially available circuit analysis software can be employed to obtain the dynamic behavior of the system.

2. Theory and Procedure

As mentioned in the previous section, the system considered consists of an electrolyte suspension of cells. The cells are modeled as spherical conductive particles surrounded by a nonconductive shell representing the membrane and by an external uniformly charged conductive shell representing the cell wall (Figure 1). The following hypotheses are, moreover, assumed on the system.

- The conductivity of the membrane is considered to be null, so the interfaces at $r = R_b$ and $r = R_c$ are impermeable to the ions. Even though biological membranes are not strictly nonconductive, their conductivity is in general very low for living cells.
- Only two types of ions are considered for every conductive medium.
- The cell wall is generally composed of a porous material that allows the exchange of ions with the external medium, and has been previously modeled as an ion-exchange resin.[22]

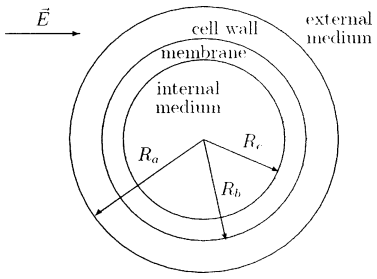

Figure 1. Model considered for the cell. The internal layer (membrane) is nonconductive, whereas all the other media are conductive. The external layer (cell wall) has an uniformly distributed density of fixed charge, and is in equilibrium with the external medium. So, the interfaces at $r = R_b$ and $r = R_c$ are impermeable to the ions, whereas the interface at $r = R_a$ is totally permeable to the ions.

* Corresponding author: e-mail: vzimmerman@herrera.unt.edu.ar
† Universidad Nacional de Tucumán.
‡ Consejo Nacional de Investigaciones Cientıficas y Técnicas.

10.1021/jp0487760 CCC: $27.50
Published on Web 07/27/2004

Consequently, the external shell is considered conductive, with an uniform distribution of fixed charges, and with the interface at $r = R_a$ perfectly permeable to the ions.

•As a consequence of the preceding hypothesis, the wall and the external medium are in equilibrium, so the valences of the mobile ions are the same in both media.

•The wall and external medium permittivities are assumed identical in order to avoid the calculation of the Born energy term in the Poisson equation.[23]

•The hydrodynamic permeability of the wall is sufficiently low to impede liquid flow in this region. However, the ions can move inside the wall (with a mobility possibly different to the ions mobility in the external medium), since it is assumed to be conductive.

•Due to a possible structure present in the internal part of the cell, the viscosity in the internal medium is considered high enough to impede the liquid flow.

•The applied electric field is weak, and as a consequence, only the linear nonequilibrium problem is solved.

According to these hypotheses, the system can be described by the following system of equations

∗Laplace equation in the membrane

$$\nabla^2\phi(\vec{r}, t) = 0, \quad R_c < r < R_b \tag{1}$$

∗Poisson equation in the internal medium, cell wall, and external medium

$$\nabla^2\phi(\vec{r}, t) = -\frac{e}{\varepsilon_o \varepsilon_j}\left(z_j^+ C^+(\vec{r}, t) + z_j^- C^-(\vec{r}, t)\right) - \overbrace{\frac{e}{\varepsilon_o \varepsilon_e} z^f C^f}^{R_b<r<R_a},$$
$$0 < r < R_c,\ R_b < r < \infty.\ j = e, i \tag{2}$$

∗Nernst−Planck equations in the internal medium, cell wall, and external medium

$$\vec{j}^{\pm}(\vec{r}, t) = -D_j^{\pm}\nabla C^{\pm}(\vec{r}, t) - \frac{e z_j^{\pm} D_j^{\pm}}{kT} C^{\pm}(\vec{r}, t)\ \nabla\phi(\vec{r}, t) + \overbrace{C^{\pm}(\vec{r}, t)\ \vec{v}(\vec{r}, t)}^{R_a<r<\infty},$$
$$0 < r < R_c,\ R_b < r < \infty.\ j = e, w, i \tag{3}$$

∗continuity equations in the internal medium, cell wall, and external medium

$$\nabla\cdot\vec{j}^{\pm}(\vec{r}, t) = -\frac{\partial C^{\pm}(\vec{r}, t)}{\partial t}, \quad 0 < r < R_c, \quad R_b < r < \infty \tag{4}$$

∗Navier−Stokes equation in the external medium

$$\eta\nabla^2\vec{v}(\vec{r}, t) - \nabla p(\vec{r}, t) = e\,(z_e^+ C^+(\vec{r}, t) + z_e^- C^-(\vec{r}, t))\ \nabla\phi(\vec{r}, t) + \rho^m\left[\frac{\partial\vec{v}(\vec{r}, t)}{\partial t} + (\vec{v}(\vec{r}, t)\cdot\nabla)\vec{v}(\vec{r}, t)\right], \quad R_a < r < \infty \tag{5}$$

∗incompressibility equation in the external medium

$$\nabla\cdot\vec{v}(\vec{r}, t) = 0, \quad R_a < r < \infty \tag{6}$$

and by the following boundary conditions:

★continuity of the potential over the whole space;

★continuity of the normal component of the displacement over the whole space;

★potential at infinity defined by the applied electric field;

★derivative of the equilibrium potential (potential without an applied field) null at the center of the particle due to the central symmetry of the system in equilibrium;

★variation of the potential induced by the applied field null at the center of the particle due to symmetry;

★field induced variations of the ion concentrations at infinity null since there is no applied concentration gradient;

★field induced variations of the ion concentrations at the center of the particle null due to symmetry;

★continuity of the normal component of the ion fluxes at the wall outer interface;

★continuity of the electrochemical potentials at the wall outer interface;

★normal components of the ion fluxes null at the membrane interfaces;

★radial component of the velocity constant at infinity;

★nonslipping condition of the solution at the wall outer interface;

★wall impermeable to the solution;

★balance of forces acting on the particle.

Here $\phi(\vec{r}, t)$ is the electric potential, $C^{\pm}(\vec{r}, t)$ is the number concentrations of positive and negative ions, $\vec{v}(\vec{r}, t)$ is the velocity of the electrolyte solution, $p(\vec{r}, t)$ is the pressure, $z_j^{\pm}$, $D_j^{\pm}$, and $\vec{j}^{\pm}(\vec{r}, t)$ are the signed valences, diffusion coefficients, and fluxes of positive and negative ions, C^f and z^f are the number concentration and signed valence of fixed charges in the wall, η and ρ^m are the viscosity and mass density of the electrolyte solution, ϵ_j and ϵ_o are the relative permittivity and permittivity of the free space, e is the elementary charge, k is the Boltzmann constant, T is the temperature, and the subindexes "e" , "w" , "m" and "i" stand for the external medium, wall, membrane, and internal medium, respectively.

The mathematical and numerical procedure followed to calculate the electric potential, ion concentration and fluid velocity, was previously described in detail in reference.[16] Using these results, the induced dipole coefficient (γ^*) and electrophoretic mobility (μ^*) are easily obtained

$$\gamma^* = \lim_{r\to\infty}\left[\frac{r^2}{R_a^3 E_o(t)}(\delta\phi(r, t) + E_o(t)r)\right] \tag{7}$$

$$\mu^* = \frac{-v_r(r\to\infty, t)}{E_o(t)} \tag{8}$$

where $E_o(t)$ is the electric field, $\delta\phi(r, t)$ is the field induced change of the electric potential, $v_r(r, t)$ is the radial component of the fluid velocity in a reference frame that instantly moves with the particle, and ω is the field angular frequency.

The permittivity (ϵ_s) and conductivity (σ_s) of the dilute suspension can be calculated using the previous results together with the Maxwell mixture formula

$$\delta\epsilon_s = \epsilon_s - \epsilon_e = 3\nu\epsilon_e\left[\mathrm{Re}\{\gamma^*\} + \frac{\sigma_e}{\omega\epsilon_o\epsilon_e}\mathrm{Im}\{\gamma^*\}\right] \tag{9}$$

$$\delta\sigma_s = \sigma_s - \sigma_e = 3\nu\sigma_e\left[\mathrm{Re}\{\gamma^*\} - \frac{\omega\epsilon_o\epsilon_e}{\sigma_e}\mathrm{Im}\{\gamma^*\}\right] \tag{10}$$

where ν is the volume concentration of cells (defined as the volume of the cells including their wall, divided by the volume of the suspension), ϵ_e and σ_e are the relative permittivity and

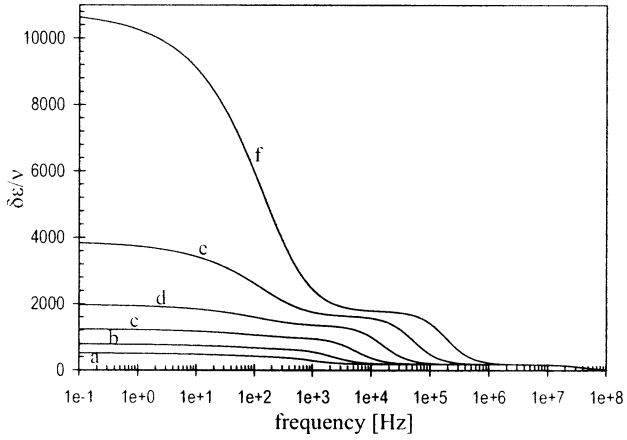

Figure 2. Permittivity spectra of cell suspensions, for different values of the product $\kappa_e R_a$: (a) 3, (b) 6, (c) 12, (d) 24, (e) 48, (f) 96. $\zeta \simeq kT/e \simeq 25$ mV; $d_w = 50$ nm. The other parameters are specified in Tables 1 and 2.

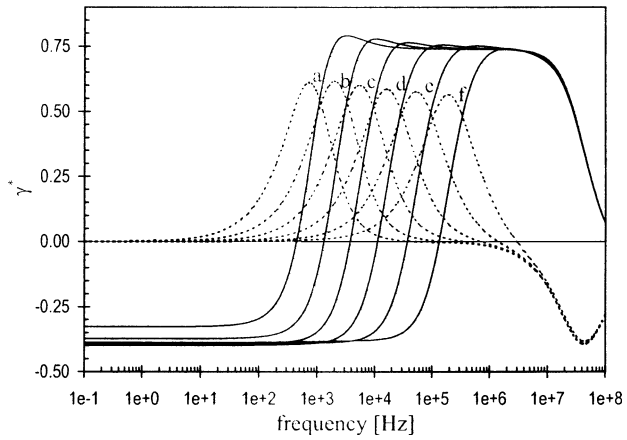

Figure 3. Spectra of the real (full lines) and imaginary (dotted lines) dipole coefficient components, for the same systems as in Figure 2.

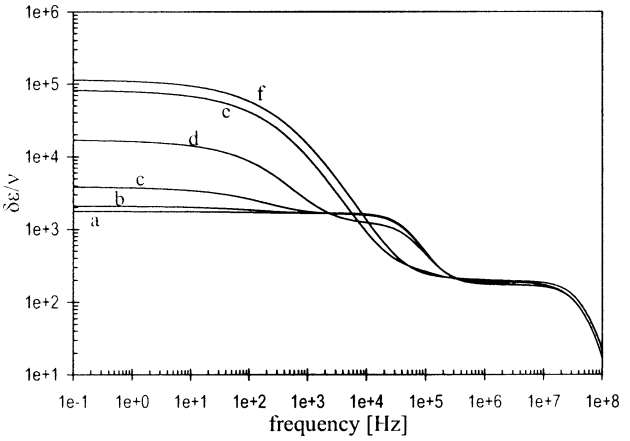

Figure 4. Permittivity spectra of cell suspensions, for different values of the ζ-potential: (a) 0.25*kT*/*e*, (b) 0.5*kT*/*e*, (c) 1*kT*/*e*, (d) 2*kT*/*e*, (e) 4*kT*/*e*, (f) 6*kT*/*e*. $\kappa_e R_a = 48$; $d_w = 50$ nm. The other parameters are specified in Tables 1 and 3.

the conductivity of the electrolyte solution, and ϵ_o is the permittivity of the free space.

3. Results and Discussion

Permittivity and dipole coefficient spectra of cells, calculated for different values of either the product $\kappa_e R_a$, the ζ-potential, or the wall thickness (h_w), are presented in Figures 2−7. κ_e is

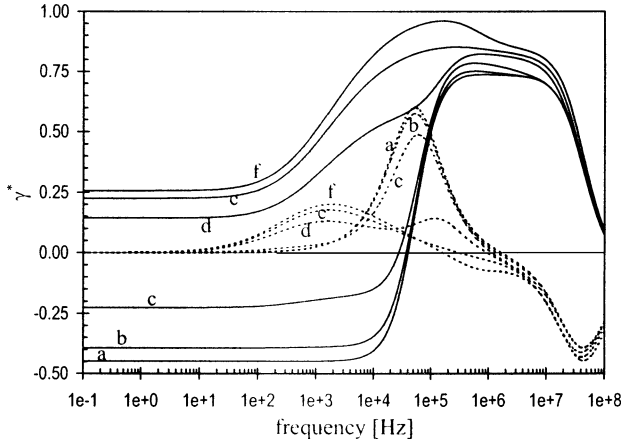

Figure 5. Spectra of the real (full lines) and imaginary (dotted lines) dipole coefficient components, for the same systems as in Figure 4.

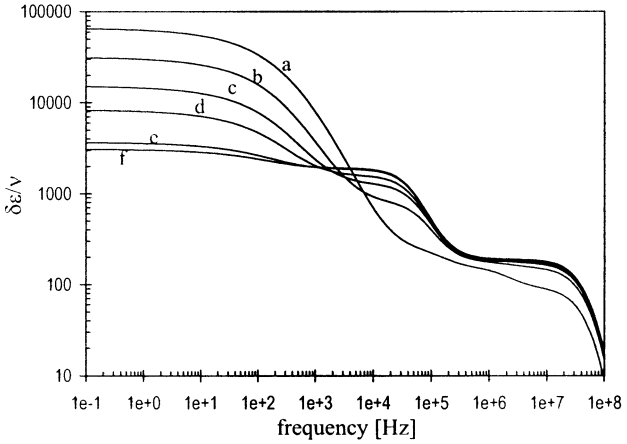

Figure 6. Permittivity spectra of cell suspensions, for different values of the wall thickness d_w (nm): (a) 300, (b) 100, (c) 50, (d) 30, (e) 10, and (f) 5. $\kappa_e R_a = 48$, $\zeta \simeq 2kT/e$. The other parameters are specified in Tables 1 and 4.

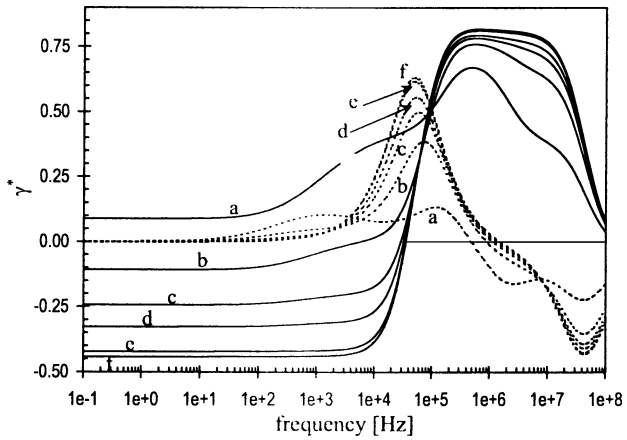

Figure 7. Spectra of the real (full lines) and imaginary (dotted lines) dipole coefficient components, for the same systems as in Figure 6.

the reciprocal Debye screening length in the external medium, and the ζ-potential is the equilibrium potential at the cell outer boundary, where the velocity of the fluid remains null with an applied field. As expected from previous works,[4,7,9,16,24] the permittivity spectra (Figures 2, 4, and 6) clearly show three dispersion regions: one at low frequencies (between 1 Hz and 1 kHz) related to the double-layer polarization and therefore to the charge of the particle (α-dispersion); a second one between 1 kHz and 1 MHz related to the process of charge of the

TABLE 1: Parameter Values Used in Figures 2−8[a]

$R_a = 1.5\ \mu m$	$\sigma_i = 0.5$ S/m	$\rho^m = 10^3$ kg/m^3
$d_w = 50$ nm	$z_e^{\pm} = z_i^{\pm} = \pm 1$	$\rho^p = 1.2 \times 10^3$ kg/m^3
$R_b - R_c = 5$ nm	$D_e^{\pm} = D_w^{\pm} =$	$\eta = 8.904 \times 10^{-4}$ Pa s
$\epsilon_e = 78.36$	$D_i^{\pm} = 2 \times 10^{-9}$ m^2/s	$T = 298.4$ K
$\epsilon_m = 4$	$z^f = 1$	
$\epsilon_i = 70$	$\phi_{eq} = 0$ V	

[a] For the full description of symbols, see ref 16.

TABLE 2: Fixed Charge Concentrations in the Wall (C^f), and Ionic Concentrations in the External Medium ($c_{e\infty}^{\pm}$) for Curves in Figures 2 and 3

	$\kappa_e R_a$	C^f (1/m^3)	$c_{e\infty}^{\pm}$ (1/m^3)
a	3	6.89×10^{21}	2.23×10^{20}
b	6	1.35×10^{22}	8.93×10^{20}
c	12	3.09×10^{22}	3.57×10^{21}
d	24	8.71×10^{22}	1.43×10^{22}
e	48	3.08×10^{23}	5.71×10^{22}
f	96	1.21×10^{24}	2.29×10^{23}

TABLE 3: Fixed Charge Concentrations in the Wall (C^f) for Curves in Figures 4 and 5

	$\zeta e/kT$	C^f (1/m^3)
a	0.25	6.18×10^{22}
b	0.5	1.30×10^{23}
c	1	3.08×10^{23}
d	2	1.05×10^{24}
e	4	8.45×10^{24}
f	6	6.28×10^{25}

TABLE 4: Fixed Charge Concentrations (C^f) and Fixed Charge (Q^f) in the Wall for Curves in Figures 6 and 7

	d_w (nm)	C^f (1/m^3)	Q^f (C)
a	300	9.52×10^{23}	1.05×10^{-12}
b	100	9.52×10^{23}	4.03×10^{-13}
c	50	9.52×10^{23}	2.08×10^{-13}
d	30	9.64×10^{23}	1.28×10^{-13}
e	10	1.30×10^{24}	5.85×10^{-14}
f	5	2.05×10^{24}	4.63×10^{-14}

membrane (β-dispersion); the third one at high frequencies (above 10 MHz) is related to the Maxwell−Wagner dispersion (δ-dispersion). In contrast, in the case of the dipole coefficient spectra (Figures 3, 5, and 7), only two dispersions can be observed in most of the curves shown in Figures, while the α-dispersion mechanism only determines the low-frequency limit of the real component of the dipole coefficient.

The spectra in Figures 2 and 3 correspond to systems with approximately the same ζ-potential and different values of the product $\kappa_e R_a$. In the high-frequency region, all the spectra coincide, since the characteristic frequency of the Maxwell−Wagner dispersion is mainly determined by the highest conductivity in the system that, for the considered cases, is the internal medium conductivity. Moreover, the amplitude does not change either, since it is independent of the conductivity for very high internal medium conductivities.[24]

For the intermediate frequency region, on the other hand, the characteristic frequency of the β-dispersion is determined by the time required to charge the membrane. This time depends on the membrane capacitance and on the conductivity of the surrounding media. However, the membrane capacitance only has a weak increase with $\kappa_e R_a$,[25] so in Figures 2 and 3, the characteristic frequency of the β-dispersion is mainly determined by the conductivity of the external medium (lowest conductivity). Hence, an increment on the external medium conductivity reduces the time of the charging process and, as a consequence, increases the characteristic frequency of the dispersion, as can be seen in the figures.

In the case of the amplitude of the β-dispersion, it is almost independent of the product $\kappa_e R_a$ for the dipole coefficient spectra (Figure 3). This amplitude is determined by the limiting high and low-frequency values of the real part of the dipole coefficient. The β-dispersion high-frequency limit is almost constant because the conductivity in the internal medium is constant and much higher than the conductivities in the wall and in the external medium.[24] In the β-dispersion low frequency limit, on the other hand, the dipole coefficient does not depend on the internal medium properties but is determined by the ratio of the wall and external medium conductivities. Even though both of these conductivities strongly change for every curve in Figure 2, their ratio remains nearly constant, leading to the very small variation that can be observed in the figure.

On the contrary, for the permittivity spectra there is a noticeable increment of the β-dispersion amplitude with $\kappa_e R_a$ (Figure 2). This increment is related to the change of the wall conductivity to external medium conductivity ratio (that decreases with $\kappa_e R_a$), and also to the previously mentioned weak increment of the effective membrane capacitance. This capacitance corresponds to a series connection of the capacitance of the bare membrane and of the capacitances of the field induced charge densities surrounding it. While the capacitances of the bare membrane and of the charge density in the internal medium do not change in Figures 2 and 3, there is a change of the field induced charge density thickness in the wall and, consequently, of the capacitance in this region. This change is due to the increment of the fixed charge density in the wall, as a consequence of the increment of the product $\kappa_e R_a$, at constant ζ-potential. An increased capacitance allows a higher value of the stored energy, which corresponds to a higher permittivity increment.

At low frequencies, the real part of the dipole coefficient decreases due to the counterion polarization. However, in view of the low value of the ζ-potential used in Figure 3, this decrement can barely be seen, as is the corresponding positive peak of the imaginary part of the dipole coefficient. Nevertheless, this last component is responsible for the strong increment of the permittivity (eq 9) since its vanishingly small value is divided by the frequency that also tends to zero. As expected, the dielectric increment strongly increases with $\kappa_e R_a$,[26] due to the increment of the fixed charge density in the wall, required in order to keep constant the ζ-potential. Moreover, Figure 2 shows that the characteristic frequency of the α-dispersion is practically independent of $\kappa_e R_a$, at least for relatively high values of this product.

The spectra in Figures 4 and 5 correspond to systems with the same value of $\kappa_e R_a$, and different values of the ζ-potential. As expected, the Maxwell−Wagner and β-dispersions do not change with the ζ-potential for low values of this parameter. However, for higher values of ζ, the excess conductivity created by the charge in the wall, screens the membrane and, consequently, hides the β-dispersion in both the dipole coefficient and the permittivity spectra.

In the low-frequency region, the ζ-potential determines the behavior of the dipole coefficient and permittivity spectra. For the dipole coefficient (Figure 5), the α-dispersion can only be observed for sufficiently high values of the ζ-potential. However, the ζ-potential determines the low-frequency limit of the dipole coefficient in all the cases.

The spectra in Figures 6 and 7 correspond to systems with the same value of $\kappa_e R_a$, the same value of the external radius

(R_a), approximately the same ζ-potential, but different values of the wall thickness (h_w). Similarly as in Figures 2 to 5, the Maxwell−Wagner dispersion does almost not change with the wall thickness since the conductivities and permittivities are the same for all the curves. However, for very thick walls (curves a and b), the internal medium becomes small, and since the Maxwell−Wagner dispersion depends on the equivalent properties of the particle rather than on the internal medium properties, a slightly different behavior in the spectra is observed. Moreover, the dispersion produced by the interface at $r = R_b$ is not hidden by the other dispersions in curves a and b and can be observed at frequencies between 1 and 10 MHz.

For the β-dispersion (frequencies between 10 kHz and 1 MHz), the characteristic frequency is almost independent of the wall thickness since both the effective membrane capacitance and the lower conductivity in the system are almost constant for all the curves. However, the amplitude of the dispersion decreases when the wall thickness increases. This is a consequence of the increment in the wall charge density, that is required in order to keep constant the ζ-potential value when the wall thickness is increased. As a result, the ratio of the wall and external medium conductivities increases with the wall thickness, screening the membrane.

Similarly as in Figures 2−5, the α-dispersion is better observed in permittivity spectra (Figure 6) than in dipole coefficient spectra (Figure 7), where it only determines the low-frequency limit of the real part of the dipole coefficient (except for curves a and b). This limit is higher for thick walls, indicating a more conductive equivalent particle. Moreover, the dielectric increment (Figure 6) also increases with the wall thickness, for the same reason.

Figure 8 shows the dependence of the permittivity spectra on the internal medium conductivity. Full and dashed lines correspond to charged and uncharged particles, respectively. In this case, the different spectra change in the frequency region related to the Maxwell−Wagner dispersion for those cases where the internal medium conductivity is higher than the conductivity of the external medium. On the other hand, the behavior for frequencies related to the β-dispersion is similar to the one observed in Figure 2.

In the low-frequency region, the spectra for charged and uncharged cells split up and the charged cells (full lines) present the additional α-dispersion. In former works that analyzed the

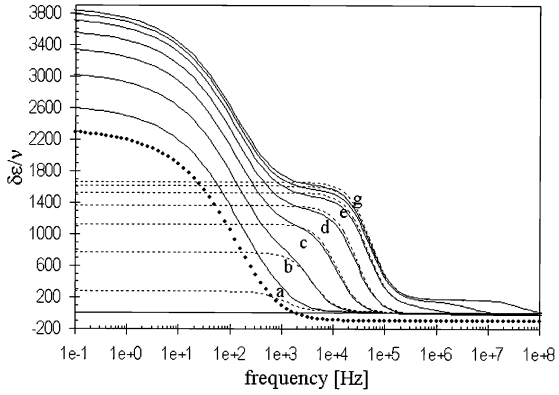

Figure 8. Permittivity spectra for suspensions of charged (full lines) and uncharged (dotted lines) cells, for different values of the internal medium conductivity; and permittivity spectrum of a homogeneous particle with a charged wall (internal medium identical to the membrane) (curve with heavy dots). σ_i [S/m] = (a) 1×10^{-5}, (b) 1×10^{-4}, (c) 5×10^{-4}, (d) 2×10^{-3}, (e) 1×10^{-2}, (f) 5×10^{-2}, and (g) 5×10^{-1}. $\kappa_e R_a = 48$, $d_w = 50$ nm, and $\zeta \simeq kT/e$ for the charged systems. The other parameters are specified in Tables 1 and 5.

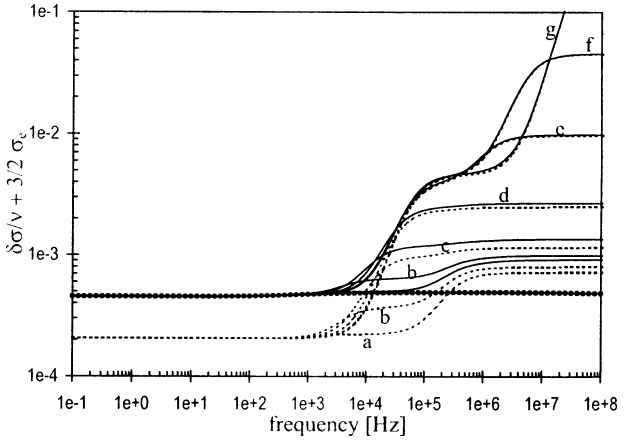

Figure 9. Same as in Figure 8 for the conductivity of the suspension (a constant was added to the conductivity in order to allow logarithmic scale).

TABLE 5: Ionic Concentrations in the Internal Medium ($c_{io}^{\pm}$) for Curves in Figures 8 and 9

	σ_i (S/m)	$c_{io}^{\pm}$ (1/m^3)
a	1×10^{-5}	4.02×10^{20}
b	1×10^{-4}	4.02×10^{21}
c	5×10^{-4}	2.01×10^{22}
d	2×10^{-3}	8.04×10^{22}
e	1×10^{-2}	4.02×10^{23}
f	5×10^{-2}	2.01×10^{24}
g	5×10^{-1}	2.01×10^{25}

dielectric spectra of cells,[4,15] it was assumed that the low-frequency region could be interpreted using the same equations as for homogeneous insulating particles with either a null internal permittivity[15] or an internal permittivity identical to that of the membrane. Our results show that even though this is correct for the dipole coefficient spectra and, therefore, for the conductivity (Figure 9), for the mobility (as previously demonstrated in ref 27), and for the electrorotation,[16] this assumption does not hold for the permittivity. This was previously analytically predicted,[24,28] and can be seen in Figure 8, comparing the different full lines with the curve with heavy dots that corresponds to a homogeneous particle surrounded by the cell wall (internal medium identical to that of the membrane). From this figure it is clear that the full spectra are obtained by adding the dispersions corresponding to each process.[24] However, this simple rule only holds for sufficiently separated processes. Moreover, it should be noted that (for sufficiently separated processes) the amplitude and characteristic frequency of the α-dispersion do not depend on the internal medium properties since, in the model considered, the membrane is nonconductive.

4. Conclusion

In this work, we present numerical results for the dielectric properties of diluted cell suspensions, calculated over a broad frequency range. We show that for typical situations where the ζ-potential is low and $\kappa_e R_a$ is not too high, the low frequency permittivity spectra strongly differ from those obtained replacing the internal medium and the membrane by a insulating homogeneous particle.

This fact is often overlooked in view that the dipole coefficient spectra of these two types of particles do coincide in the low-frequency range. Because of this, the low-frequency conductivity and electrophoretic mobility spectra do not depend on the dielectric properties of the particle. The reason the permittivity behaves differently can be understood on the basis

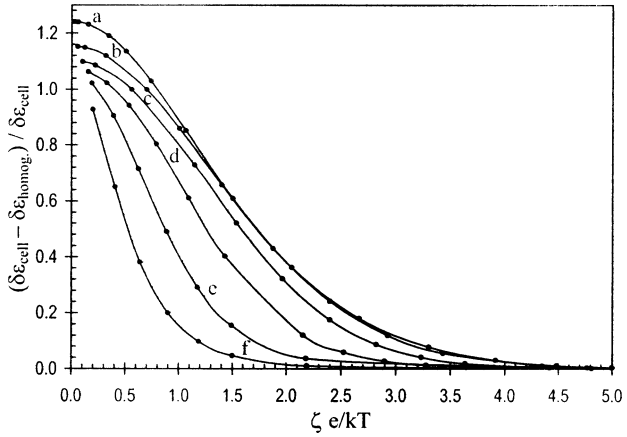

Figure 10. Difference between the permittivity of a suspension of cells and a suspension of homogeneous particles surrounded by a wall divided by the permittivity of the cell suspension, as a function of the ζ-potential, and calculated for different values of the product $\kappa_e R_a$: (a) 3, (b) 6, (c) 12, (d) 24, (e) 48, (f) 96. The other parameters are specified in Table 1.

of the relationship between the permittivity and the stored energy. At low frequencies, the electric field (and therefore the dipole coefficient) around a cell is the same as around an insulating homogeneous particle surrounded by the same wall. However, under these conditions the cell carries a fully charged membrane and stores, consequently, more energy.

It is important to note, finally, that the interpretation of the low-frequency permittivity spectra of cells using the homogeneous particle theory, does not always lead to wrong results: it all depends on the ζ-potential and $\kappa_e R_a$ values. This can be seen in Figure 10, where the difference between the low-frequency permittivity of a suspension of cells and a suspension of homogeneous particles surrounded by a wall (divided by the permittivity of the cell suspension) is presented as a function of the ζ-potential, and calculated for different values of $\kappa_e R_a$. As can be seen, the homogeneous particle model can be satisfactorily used for cells when the $\kappa_e R_a$ and the ζ-potential values are sufficiently high.

Acknowledgment. This work was partially supported by Grant 26/E220 of the Consejo de Investigaciones de la Universidad Nacional de Tucumán.

References and Notes

(1) Carstensen, E. L. *Biophys. J.* **1967**, *7*, 493−503.
(2) Fuhr, G.; Kuzmin, P. I. *Biophys. J.* **1986**, *50*, 789−795.
(3) Fuhr, G.; Hagedorn, R. Cell electrorotation. In *Electrical Manipulation of cells*; Lynch, P., Davey, M., Eds.; Chapman and Hall: New York, 1996.
(4) Schwan, H. P. *Ferroelectrics* **1988**, *86*, 205−223.
(5) Arnold, W. M.; Zimmermann, U. *Z. Naturforsch.* **1982**, *37*, 908−915.
(6) Arnold, W. M.; Zimmermann, U. *J. Electrostat.* **1988**, *21*, 151−191.
(7) Foster, K. R.; Schwan, H. P. *CRC Crit. Rev. Biomed. Eng.* **1989**, *17*, 25−104.
(8) Asami, K.; Yonezawa, T. *Biophys. J.* **1996**, *71*, 2192−2200.
(9) Hölzel, R. *Biophys. J.* **1997**, *73*, 1103−1109.
(10) Einolf, C. W., Jr.; Carstensen, E. L. *Biophys. J.* **1969**, *9*, 634−643.
(11) Foster, K. R.; Sauer, F. A.; Schwan, H. P. *Biophys. J.* **1992**, *63*, 180−190.
(12) Zhou, X.-F.; Markx, G. H.; Pethig, R.; Eastwood, I. M. *Biochim. Biophys. Acta* **1995**, *1245*, 85−93.
(13) Neu, B.; Georgieva, R.; Bäumler, H.; Shilov, V. N.; Knippel, E.; Donath, E. *Colloids Surf. A* **1998**, *140*, 325−332.
(14) Georgieva, R.; Neu, B.; Shilov, V. N.; Knippel, E.; Budde, A.; Latza, R.; Donath, E.; Kiesewetter, H.; Bäumler, H. *Biophys. J.* **1998**, *74*, 2114−2120.
(15) van der Wal, A.; Minor, M.; Norde, W.; Zehnder, A. J.; Lyklema, J. *J. Colloid Interface Sci.* **1997**, *186*, 71−79.
(16) Zimmerman, V.; Grosse, C.; Shilov, V. N. *J. Phys. Chem. B* **2003**, *107*, 14612−14621.
(17) López-Garcıa, J. J.; Horno, J.; González-Caballero, F.; Grosse, C.; Delgado, A. V. *J. Colloid Interface Sci.* **2000**, *228*, 95−104.
(18) Horno, J.; González-Fernández, C.; Hayas, A.; González-Caballero, F. *Biophys. J.* **1989**, *55*, 527−535.
(19) Shilov, V. N.; Delgado, A. V.; González-Caballero, F.; Horno, J.; López-Garcıa, J. J.; Grosse, C. *J. Colloid Interface Sci.* **2000**, *232*, 141−148.
(20) López-Garcıa, J. J.; Horno, J.; Delgado, A. V.; González-Caballero, F. *J. Phys. Chem. B* **1999**, *103*, 11297−11307.
(21) Zimmerman, V.; Shilov, V. N.; López-Garcıa, J. J.; Grosse, C. *J. Phys. Chem. B* **2002**, *106*, 13384−13392.
(22) Einolf, C. W., Jr.; Carstensen, E. L. *J. Phys. Chem.* **1971**, *75*, 1091−1099.
(23) Born, M. *Z. Physik* **1920**, *1*, 45−48.
(24) Grosse, C. Relaxation mechanisms of homogeneous particles and cells suspended in aqueous electrolyte solutions. In *Interfacial Electrokinetics and electrophoresis*, Vol. 106. Delgado, A. V., Ed.; Marcel Dekker: New York, 2002.
(25) Garcıa, A.; Barchini, R.; Grosse, C. *J. Phys. D: Appl. Phys.* **1985**, *18*, 1891−1896.
(26) Grosse, C.; Arroyo, F.; Shilov, V. N.; Delgado, A. V. *J. Colloid Interface Sci.* **2001**, *242*, 75−81.
(27) O'Brien, R. W.; White, L. R. *J. Chem. Soc., Faraday Trans.* **1978**, *74*, 1607−1626.
(28) Simonov, I.; Shilov, V. N. *Kolloidnij Zh.* **1977**, *39*, 878−884.